The role of 6-phosphogluconate dehydrogenase in vascular smooth muscle cell phenotypic switching and angioplasty-induced intimal hyperplasia

Amy L. Lu,[a,b] Li Yin, PhD,[a,c,d] Yitao Huang, BS,[a] Zain Husain Islam,[a] Rohan Kanchetty,[a] Campbell Johnston,[a] Kaijie Zhang, MD,[a,c,d] Xiujie Xie, PhD,[b] Ki Ho Park, PhD,[a] Charles E. Chalfant, PhD,[b,e] *and* Bowen Wang, PhD,[a,d] *Charlottesville and Richmond, VA; Zhejiang, China; and Chicago, IL*

ABSTRACT

Background: Restenosis poses a significant challenge for individuals afflicted with peripheral artery diseases, often leading to considerable morbidity and necessitating repeated interventions. The primary culprit behind the pathogenesis of restenosis is intimal hyperplasia (IH), in which the hyperproliferative and migratory vascular smooth muscle cell (VSMC) accumulate excessively in the tunica intima. 6-Phosphogluconate dehydrogenase (6PGD), sometimes referred to as PGD, is one of the critical enzymes in pentose phosphate pathway (PPP). In this study, we sought to probe whether 6PGD is aberrantly regulated in IH and contributes to VSMC phenotypic switching.

Methods: We used clinical specimens of diseased human coronary arteries with IH lesions and observed robust upregulation of 6PGD at protein level in both the medial and intimal layers in comparison with healthy arterial segments.

Results: 6PGD activity and protein expression were profoundly stimulated upon platelet-derived growth factor-induced VSMC phenotypic switching. Using gain-of-function (dCas9-mediated transcriptional activation) and loss-of-function (small interfering RNA-mediated) silencing, we were able to demonstrate the pathogenic role of 6PGD in driving VSMC hyperproliferation, migration, dedifferentiation, and inflammation. Finally, we conducted a rat model of balloon angioplasty in the common carotid artery, with Pluronic hydrogel-assisted perivascular delivery of *Physcion*, a selective 6PGD inhibitor with poor systemic bioavailability, and observed effective mitigation of IH.

Conclusions: We contend that aberrant 6PGD expression and activity—indicative of a metabolic shift toward pentose phosphate pathway—could serve as a new disease-driving mechanism and, hence, an actionable target for the development of effective new therapies for IH and restenosis after endovascular interventions. (JVS—Vascular Science 2024;5:100214.)

Keywords: Restenosis; Intimal hyperplasia; Smooth muscle cell; Peripheral vascular disease; Pentose phosphate pathway

Despite advances in surgical techniques and medical devices, endovascular interventions for cardiovascular and peripheral vascular diseases, such as percutaneous transluminal angioplasty and stenting, frequently encounter failure owing to the renarrowing of the reconstructed vessel, known as restenosis. In the current era of drug-eluting devices, the prevalence of postintervention restenosis is estimated approximately 10% to 55% of patients after percutaneous coronary intervention and can be as high as 70% in the lower extremities.[1,2] Intimal hyperplasia (IH) stands out as the primary culprit behind the pathogenesis of restenosis, characterized by the excessive accumulation of hyperproliferative and migratory vascular smooth muscle cell (VSMCs) in the tunica intima.[3] After endovascular injury and subsequent exposure to numerous cytokines and growth factors, VSMCs could undergo phenotypic switching from a healthy, quiescent state to a proliferative, migratory, dedifferentiated, and synthetic phenotype.[4,5] Such phenotypic switching of VSMCs has been documented widely in literature as the key disease driver behind a myriad of cardiovascular pathologies, including restenosis, IH, aortic aneurysm, and atherosclerosis.[3,6,7] A growing body of research evidence indicates the importance of targeting VSMC phenotypic switching in the effective management of these vascular diseases.[4,8]

Emerging studies have suggested an important link between cellular metabolism and VSMC phenotypic switching.[9,10] The metabolic shift between oxidative phosphorylation and glycolysis in VSMCs was interrogated recently, revealing a profound impact of the

From the Department of Surgery, School of Medicine,[a] Division of Hematology & Oncology, Department of Medicine,[b] University of Virginia, Charlottesville; the Department of Vascular Surgery, Second Affiliated Hospital of Zhejiang University School of Medicine, Zhejiang[c]; the Department of Surgery, Feinberg School of Medicine, Northwestern University, Chicago[d]; and the Research Service, Richmond Veterans Administration Medical Center, Richmond.[e]

AL and LY contributed equally to this article and share co-first authorship.

CC and BW contributed equally to this article and share senior authorship.

Additional material for this article may be found online at www.jvsvs.org.

Correspondence: Bowen Wang, PhD, Department of Surgery, Feinberg School of Medicine, Northwestern University, 300 E Superior 2-709, Chicago, IL 60611 (e-mail: bowenwang@northwestern.edu).

The editors and reviewers of this article have no relevant financial relationships to disclose per the JVS-Vascular Science policy that requires reviewers to decline review of any manuscript for which they may have a conflict of interest.

2666-3503

https://doi.org/10.1016/j.jvssci.2024.100214

Warburg effect—increased use of glucose and accumulation of lactate via aerobic glycolysis for energy production—in fueling the hyperproliferative and migratory phenotypic switching of VSMCs.[9-13] However, the biological and pathophysiological implications of the pentose phosphate pathway (PPP), an alternative route for glucose oxidation in parallel to glycolysis, are largely unknown in the context of VSMC. PPP is critical in maintaining redox and carbon homeostasis, as well as the biosynthesis of nucleotides and amino acids. Data derived from cultured VSMCs and transgenic rats with PPP defects suggest a disease-promoting role of the PPP metabolism in VSMC phenotypic switching, with the primary focus on the first rate-limiting enzyme glucose-6-phosphate dehydrogenase (G6PD).[14-17] However, little is known about the mechanistic and therapeutic implications of the PPP and its other key enzymes in VSMCs.

6-Phosphogluconate dehydrogenase (6PGD), sometimes referred to as PGD, is the third oxidative decarboxylase and the only other nicotinamide adenine dinucleotide phosphate-producing enzyme in PPP. Thus far, our knowledge of its role in the cardiovascular system remains elusive. A recent study unveiled the association between increased 6PGD expression levels and atherosclerotic plaque stability based on metabolomics and bulk transcriptomic data from endarterectomies, whereas the exact cellular contributions are unknown.[18] In the current study, we sought to probe whether 6PGD is regulated in IH with a special focus on VSMC. We hypothesized that 6PGD of the PPP metabolism is upregulated aberrantly upon endovascular injury, which critically contributes to VSMC phenotypic switching and hence the development of IH.

METHODS

Materials. All research materials and vendor information are summarized in Table I. Human aortic smooth muscle cells (AoSMCs, CC-2571), smooth muscle cell basal medium (SmBM, CC-3181), and SmBM plus SingleQuots of supplements (CC-3182) were purchased from Lonza (Basel, Switzerland). PDGF-BB (520-BB) was from R&D Systems (Minneapolis, MN). Cell Titer-Glo 2.0 Assay kit (G9242) was from Promega (Madison, WI). The PGD activity assay kit was from Abcam (Cambridge, UK) (ab241016). Transwell (12-mm diameter, 3.0 μm pore size) Polycarbonate Membrane Insert was from Corning (Corning, NY) (3402). The following products were from Thermo Fisher Scientific (Waltham, MA): Silencer Select Negative Control No.1 small interfering RNA (siRNA) (4390844) or Silencer select siRNA-PGD (4390824, ID: s10394 and s10395), Opti-MEM I Reduced Serum Medium (31985062), Lipofectamine RNAiMAX Transfection Reagent (13778150), TaqMan primers (6PGD, Assay ID: Hs00427230_m1; glyceraldehyde 3-phosphate dehydrogenase (GAPDH), Assay ID: Hs02786624_g1), PGD polyclonal antibody (PA5-83188), High-Capacity complementary DNA (cDNA) Reverse Transcription kit (4368814), TaqMan Universal Master Mix II (4440043), Halt Protease and Phosphatase Inhibitor Cocktail (78440), Pierce BCA Protein Assay kit (23227). Control Lentiviral Activation Particles (Santa Cruz Biotechnology, Dallas, TX; sc-437282) or PGD synthase Lentiviral Activation Particles (Santa Cruz, sc-405437-LAC-2). The polybrene was from Millipore Sigma (Burlington, MA) (TR-1003-G). The following antibodies were from Cell Signaling Technology (Danvers, MA): Phospho-p44/42 MAPK (4370S), p44/42 MAPK (4695S), Phospho-MEK1/2 (9154S), MEK1/2 (9122S), and GAPDH (2118S).

Human coronary artery sections. Deidentified human coronary artery specimens (in the form of formalin-fixed paraffin-embedded sections) from four donors were provided by the CVPath Institute, through its study protocol approved for exempt review by the institutional review board of the CVPath Institute as described by other users/study teams and ours.[19,20] For each donor, coronary arteries were collected during autopsy examinations, and both diseased (left anterior descending arteries with extensive IH) and healthy (mid-right coronary arteries with none or minimal IH) arterial sections were identified by CVPath Institute's pathology team. The donors' sex, race, and age are summarized in Table II.

Human AoSMC culture. Cell cultures were maintained in a humidified incubator at 37 °C with 5% CO_2 following previously established protocols.[21,22] AoSMCs were cultured in SmBM supplemented as mentioned earlier. Passaging of cells at a 1:4 ratio occurred every 3 to 4 days. All experiments were conducted using AoSMC between passages 5 and 8.

6PGD activity assay. 6PGD activity was conducted following manufacture's protocol. Harvested cells were lysed in assay buffer and subsequently centrifuged at 10,000×*g* for 20 minutes. The resulting supernatant was carefully transferred to a fresh tube for the assay. To prepare the reaction mix, combine PGD assay buffer, 6PGD developer, and substrate. We added 50 μL of the Reaction Mix to each well containing the standard, positive control, and test samples. We measured absorbance promptly at 460 nm in kinetic mode for 45 to 60 minutes at 37°C.

Quantitative real-time polymerase chain reaction. Total RNA was isolated from cell lysates using the TRIzol reagent. Subsequently, cDNA synthesis was performed using the High-Capacity cDNA Reverse Transcription kit (4368814). Each 20-μL reaction involved amplifying 10 ng of cDNA through quantitative real-time polymerase chain reaction with TaqMan Universal Master Mix II. Messenger RNA (mRNA) expression levels were assessed using the Applied Biosystems 7900HT Fast Real-Time

Table I. Summary of materials

Source	Cat#	Name
Lonza	CC-2571	Human AoSMCs
Lonza	CC-3181	SmBM
Lonza	CC-3182	SmBM plus SingleQuots of supplements
R&D Systems	520-BB	PDGF-BB
Promega	G9242	Cell Titer-Glo 2.0 Assay kit
Abcam	ab241016	PGD activity assay kit
Abcam	ab176749	Apoptosis/Necrosis Assay Kit
Corning	3402	Transwell Polycarbonate Membrane Insert
Thermo Fisher Scientific	4390844	Silencer Select Negative Control No.1 siRNA
Thermo Fisher Scientific	4390824	Silencer select siRNA-PGD. ID: s10394 and s10395
Thermo Fisher Scientific	31985062	Opti-MEM I Reduced Serum Medium
Thermo Fisher Scientific	13778150	Lipofectamine RNAiMAX Transfection Reagent
Thermo Fisher Scientific	Hs00427230_m1	TaqMan primers: 6PGD
Thermo Fisher Scientific	Hs02786624_g1	TaqMan primers: GAPDH
Thermo Fisher Scientific	Hs05032285_s1	TaqMan primers: α-SMA
Thermo Fisher Scientific	Hs00167476_m1	TaqMan primers: ALDH1A3
Thermo Fisher Scientific	Hs00164932_m1	TaqMan primers: ICAM1
Thermo Fisher Scientific	PA5-83188	PGD polyclonal antibody
Thermo Fisher Scientific	4368814	High-Capacity cDNA Reverse Transcription kit
Thermo Fisher Scientific	4440043	TaqMan Universal Master Mix II
Thermo Fisher Scientific	78440	Halt Protease and Phosphatase Inhibitor Cocktail
Thermo Fisher Scientific	23227	Pierce BCA Protein Assay kit
Thermo Fisher Scientific	A21207	Donkey anti-Rabbit IgG (H + L) Highly Cross-Adsorbed Secondary Antibody, Alexa Fluor 594
Thermo Fisher Scientific	A11001	Goat anti-Mouse IgG (H + L) Cross-Adsorbed Secondary Antibody, Alexa Fluor 488
Santa Cruz	sc-437282	Control Lentiviral Activation Particles
Santa Cruz	sc-405437-LAC-2	PGD synthase Lentiviral Activation Particles
Millipore Sigma	TR-1003-G	polybrene
Cell Signaling Technology	4370S	Phospho-p44/42 MAPK
Cell Signaling Technology	4695S	p44/42 MAPK
Cell Signaling Technology	9154S	Phospho-MEK1/2
Cell Signaling Technology	9122S	MEK1/2
Cell Signaling Technology	2118S	GAPDH
Cell Signaling Technology	75262SF	Phospho-MEK1/2
Cell Signaling Technology	56856S	aSMA
NOVUS	NB100-82088	Phospho-p65

AoSMC, Aortic smooth muscle cell; *cDNA*, complementary DNA; *GAPDH*, glyceraldehyde 3-phosphate dehydrogenase; *6PGD*, 6-Phosphogluconate dehydrogenase; *PDGF-BB*, platelet-derived growth factor; *SmBM*, smooth muscle cell basal medium.

polymerase chain reaction System with Taqman primers. Data were quantified using the ΔΔCt method. The 6PGD mRNA level was normalized to GAPDH.

Western blotting. Western blotting was conducted as previously described.[23] Cells were lysed in RIPA buffer supplemented with Halt Protease and Phosphatase Inhibitor Cocktail (78440). The Pierce BCA Protein Assay kit (23227) was used for determining protein concentrations. Whole-cell lysates were combined with Laemmli loading buffer, subjected to boiling, separated through 4% to 20% SDS-PAGE, and then transferred onto a

Table II. Summary of deidentified donor information from the CVPath Institute

Case number	Age, years	Race	Sex
1	87	Caucasian	Female
2	79	Caucasian	Male
3	81	Caucasian	Male
4	83	Caucasian	Male

polyvinylidene fluoride membrane. After this, immunoblot analyses were conducted using specific antibodies. Visualization of the specific protein bands was achieved using the Western Blotting Kit (Pierce, 35050).

Treatment of AoSMCs with *Physcion*, siRNA, and/or cytokines. In vitro experiments involving chemical compound, siRNA, and cytokine were conducted as previously described.[23] AoSMCs were cultured in full medium until reaching 60% to 80% confluency. Subsequently, the medium was changed to basal medium without fetal bovine serum for 24 hours. After this, cells were treated with *Physcion*/control or transfected with si-6PGD/scrambled control using Lipofectamine RNAiMAX Transfection Reagent for an additional 24 hours. The culture was then incubated with fresh basal medium (without Lipofectamine), with or without PDGF-BB (40 ng/mL). Cells were harvested for assays 24 hours after the cytokine treatment.

dCas9-synergistic activation mediator-mediated 6PGD gain-of-function in AoSMCs. AoSMCs were cultured in full medium until reaching 50% to 60% confluency and subsequently switched to basal medium (0% fetal bovine serum) for 2 hours. The cells were then infected with lentivirus (sc-437282 or sc-405437-LAC-2) at a multiplicity of infection of 2 for 12 hours, followed by a change to full medium. After an additional 36-hour incubation, the cells were collected for downstream assays.

Cell Titer-Glo viability assay. AoSMC viability was determined using Cell Titer-Glo luminescent assay, as previously described.[22,23] To assess cell proliferation, the Cell Titer-Glo Luminescent Cell Viability kit was used following the manufacturer's guidelines. Cells were initially seeded in 96-well plates at a density of 2000 cells per well. At 48 hours after treatment with *Physcion* with or without PDGF-BB, siRNA with or without PDGF-BB, or lentivirus, the plates were decanted carefully and refilled with 50 μL of Cell Titer-Glo reagent and 50 μL of phosphate-buffered saline (PBS) per well. Following a 10-minute incubation at room temperature in the dark, luminescence readings were taken using the Gene5 Multi-Mode Microplate Reader (Molecular Devices, Sunnyvale, CA) with a 250-ms integration.

Transwell migration assay. Migration assay was conducted following a previously established protocol.[21,24] AoSMCs were cultured in 12-well transwell upper inserts until reaching 70% to 80% confluence. After 24 hours of starvation in basal medium, the cells were used for subsequent experiments. In the knockdown experiment, cells were transfected with siRNA or a scrambled control. For overexpression, cells were infected with lentivirus carrying control or 6PGD. In inhibitor treatment, cells were exposed to *Physcion* or a vehicle control. Full growth medium was added to the lower chamber. After a 24-hour incubation period (cell migration), the inserts were washed three times with PBS. The cells on the inside of the Transwell inserts were removed using cotton swabs. The cells on the lower surface of the membrane were stained with 0.1% crystal violet (20% methanol) for 20 minutes. The insert was washed three times with PBS to remove unbound crystal violet and then air dried. The migrated cells were imaged under a microscope, and 400 μL of 33% (v/v) acetic acid was added to the insert and shaken for 10 minutes to elute the bound crystal violet. The eluent from the lower chamber was measured for absorbance (590 nm) using a 96-well microplate reader.

Balloon angioplasty procedure in rat carotid arteries. All studies involving animals were in accordance to the Guide for the Care and Use of Laboratory Animals.[25] The animal study protocol was approved by the Animal Care and Use Committee at the University of Virginia (Protocol#4327). Balloon angioplasty in common carotid arteries was performed in male Sprague-Dawley rats (300-350 g) as described previously.[23,26] In brief, the rats were anesthetized with isoflurane (5% for induction and 2%-3% for maintenance). After preparing the skin, a midline neck incision was made. After exposing the left common carotid artery, the branches of the artery were looped to avoid blood reflux. A 2F Fogarty embolectomy catheter (Edward Life Science, Irvine, CA) was inserted through an arteriotomy on the external carotid artery to injure the endothelium of the vessel. The balloon catheter was inflated at 1.5 atm and then withdrawn until the catheter reached the carotid bifurcation. After three times of withdrawals, we included a fourth cycle with concomitant rotation of the catheter during withdrawal. This minor modification (fourth insertion with rotation) was introduced in our recent studies to improve the consistency of complete endothelium denudation, animal-to-animal variations in terms of the intima area vs media area (I/M) ratio, and neointima centricity.[20,27] The external carotid artery was ligated permanently before resuming the blood flow and wound closure. Throughout the procedure, the rat was kept anesthetized via isoflurane, inhaling at a flow rate of 2 to 4 L/min. Carprofen and a slow-release form of bupivacaine (Nocita) were injected subcutaneously per institutionally approved analgesic plans. Two weeks after the procedure, the common

carotid arteries were collected. The animals were anesthetized with isoflurane and the arteries were collected after perfusion fixation at a physiological pressure of 100 mm Hg.

Hydrogel-mediated perivascular *Physcion* delivery. Pluronic F127 hydrogel was used to deliver *Physcion* locally around carotid artery, as described in our previous studies.[28-30] Briefly, *Physcion* and its vehicle control, dimethylformamide, were mixed in 25% Pluronic gel maintained at 4°C throughout the whole process. Immediately after carotid artery balloon angioplasty in male Sprague-Dawley rats, the hydrogel/*Physcion* mixture (10 mg/kg payload) was administered around the injured common carotid artery to achieve a localized sustained release over the course of 2 to 3 days.

Histological and morphometric analyses. Paraffin cross-sections (5 μm thick) were cut at equally spaced intervals using a microtome (Leica, Wetzlar, Germany). For morphometric analysis of IH analysis, the slides were stained with hematoxylin and eosin. Morphometric parameters were measured on the sections and calculated using ImageJ software: lumen area, the area inside internal elastic lamina (IEL area), the area inside external elastic lamina (EEL area), intima area (= IEL area − lumen area), and media area (= EEL area − IEL area). IH, the I/M ratio was calculated by (IEL area − lumen area)/(EEL area − IEL area). We collected three to four sections from different segments of each common carotid artery (from individual rat) and measured them; the measurements were pooled from all sections to generate a mean value for each animal. The mean values from all the animals in each treatment group were averaged, and then the standard error of the mean was calculated. All the measurements were performed by an independent researcher who was blinded to the experimental treatment.

Immunohistochemistry and immunofluorescence staining. IHC was conducted following our previously established protocols.[31,32] In summary, paraffin-embedded arteries were sectioned into 5-μm slices. Slides underwent deparaffinization and rehydration through xylenes and a graded alcohol series. Antigen retrieval was performed in citrate buffer using a decloaking chamber (NxGen, Biocare Medical, Pacheco, CA) at 80 °C for 2 hours. Endogenous peroxidase activity was blocked by incubation with 3% H_2O_2 for 15 minutes. Immunostaining of 6PGD, or phosphorylated-ERK, phosphorylated-MEK, and P-P65 was accomplished using the ImmPRESS HRP anti-Rabbit IgG (Peroxidase) Polymer Detection Kit (Vector Laboratories, Burlingame, CA; MP-7451-15) along with primary antibodies. Visualization was achieved using ImmPACT DAB Peroxidase (HRP) Substrate. At least three fields in each section were captured for analysis.

For immunofluorescence staining, formalin-fixed paraffin-embedded sections were deparaffinized and subjected to antigen retrieval as described above, followed by incubation with primary antibodies and appropriate fluorophore-conjugated secondary antibodies (detailed information listed in Table I). Images were then acquired using EVOS M7000 and STELLARIS 5 confocal point scanning system with Leica DMi8 inverted microscope.

Apoptosis/necrosis assay. We seeded 3×10^4 cells in each well of a 96-well microplate (black wells with a clear flat bottom). After transfection with Scramble or siRNA, transduction with lentiviral control or 6PGD, or treatment with *Physcion* or vehicle control, an apoptosis assay was performed 48 hours later. Cells were washed twice with 100 μL of Assay Buffer. After washing, 200 μL of Assay Buffer, 2 μL of Apopxin Green Indicator, and 1 μL of 7-AAD were added to the cells. After incubation at room temperature for 30 to 60 minutes, the cells were washed twice with 100 μL of Assay Buffer and then replaced with 100 μL of fresh Assay Buffer for analysis using a fluorescence microscope. Apoptotic cells, showing green staining were using the fluorescein isothiocyanate channel (Ex/Em = 490/525 nm). Cell viability was analyzed using the Texas Red channel (Ex/Em = 550/650 nm) and the violet channel (Ex/Em = 405/450 nm).

Statistical analysis. We used Prism 9.0 (GraphPad Software) for the statistical analyses. Comparisons between experimental groups were assessed using one-way analysis of variance (for multiple groups) or the Student *t* test (for two groups), as indicated in the figure legends. Data are expressed as mean ± standard error of the mean from independent replicate experiments or as mean ± standard deviation from replicates. *P* values of $<.05$ were regarded as statistically significant.

RESULTS

PPP enzyme 6PGD is upregulated aberrantly in the intimal and medial layers of restenotic human coronary arteries. Recent evidence suggests aberrant PPP activity to be implicated in atherosclerosis and plaque instability, whereas loss-of-function of PPPs first speed-limiting enzyme, G6PD, partially averted VSMC phenotypic switching.[14] Whether 6PGD, the third enzyme of the PPP branch, is activated aberrantly and/or upregulated in occlusive vasculopathies, such as atherosclerosis and IH, remains unknown. Herein, we conducted immunohistological staining of 6PGD in human coronary arteries with or without IH. Tissue specimens were acquired from CVPath Institute as previously used in our study.[20] As shown in Fig 1, *A*, healthy coronary artery sections, featuring no to minimal IH, displayed positive staining of 6PGD at a moderate intensity in both intimal and medial layers, whereas no positive cells

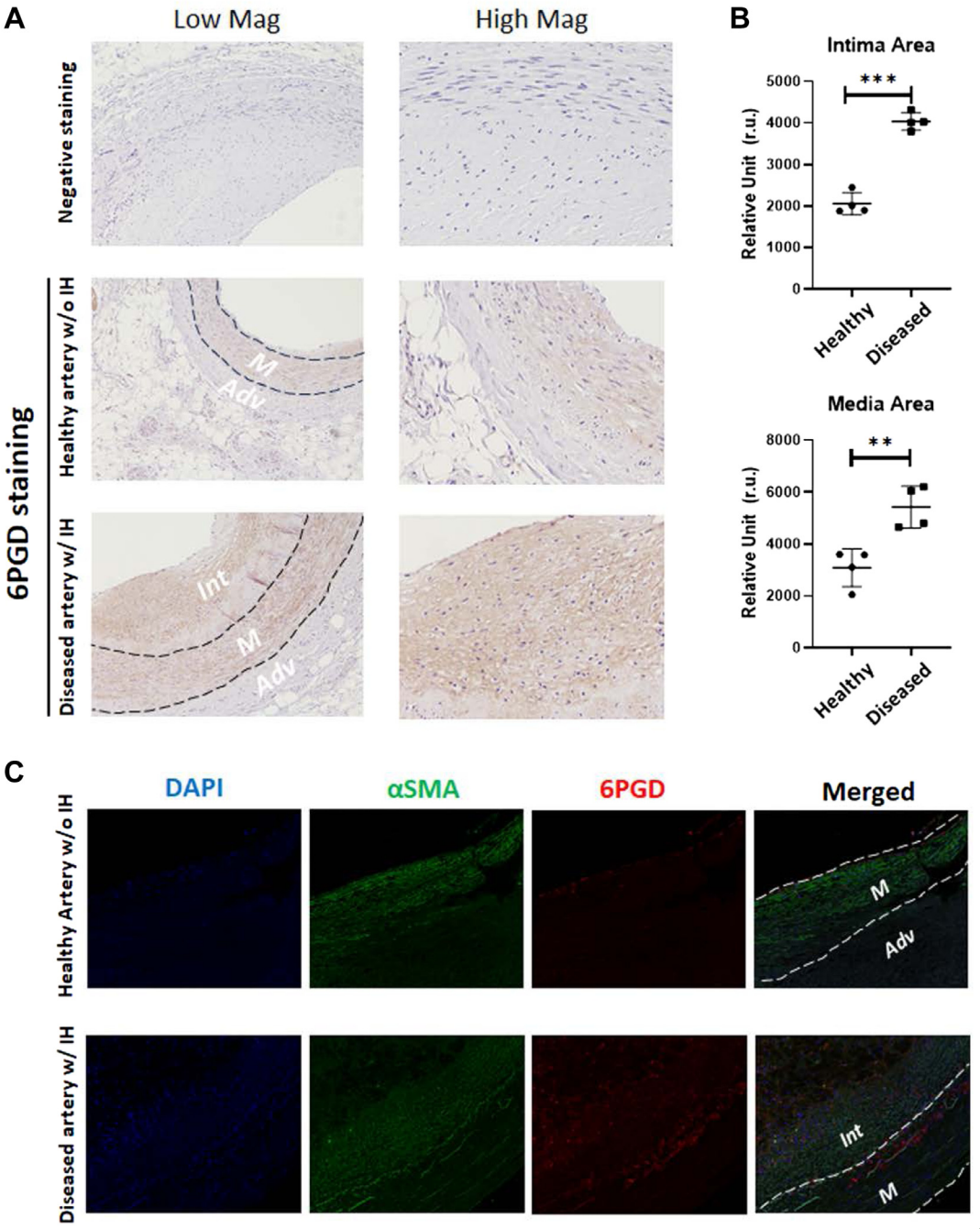

Fig 1. Pentose phosphate pathway (PPP) enzyme 6-phosphogluconate dehydrogenase (*6PGD*) is upregulated aberrantly in the neointimal layer of diseased human coronary arteries with extensive intimal hyperplasia (IH). **(A)** Representative immunohistochemical staining of 6PGD in cross-sections from human coronary arteries with or without severe IH lesions. Negative control staining followed the same procedures, with the exception that the primary antibody was omitted. Dashed lines highlight the internal and external elastic laminae (EEL). Tunica intima (*Int*), media (*M*), and adventitia (*Adv*) are annotated, respectively. **(B)** The quantification of 6PGD expression level in tunica intima area and tunica media area. Positive staining was assessed based on colorimetric intensity per image field, quantified by averaging three sections from each sample. The resulting averages from all four unique donors (each including healthy vs diseased arterial segments with severe IH) were then further averaged, as illustrated in the scatter plots. **(C)** Representative confocal images of 6PGD (red channel) and vascular smooth muscle cell (VSMC) marker α smooth muscle actin (*α-SMA*) (green channel) costaining in healthy vs diseased (with IH lesions) human coronary arteries. Student *t* test: $^{**}P < .01$, $^{***}P < .001$. *Mag*, magnification.

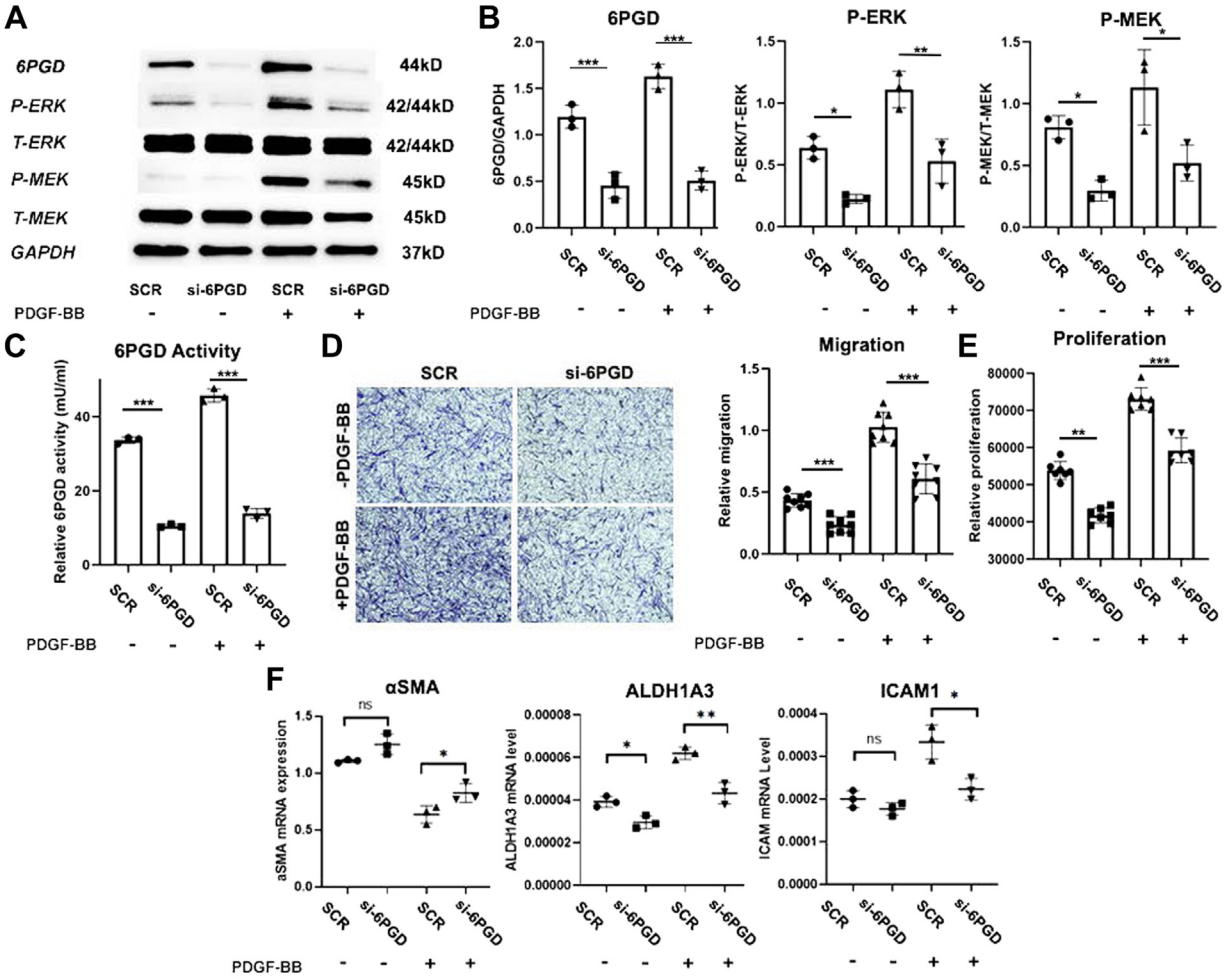

Fig 2. 6-Phosphogluconate dehydrogenase (*6PGD*) silencing diminishes 6PGD enzyme activity and blocks vascular smooth muscle cell (VSMC) phenotypic switching and ERK/MEK signaling in VSMCs in vitro. Primary culture of human aortic smooth muscle cells (AoSMCs) were subjected to serum starvation for 24 hours before the treatment with 6PGD-specific small interfering RNA (*si-6PGD*) or scramble control (*SCR*). After 24 hours of treatment, platelet-derived growth factor (PDGF-BB) was introduced to induce AoSMC dysfunction for an additional 24 hours. **(A** and **B)** Representative Western blot images and protein-level quantitation of phosphorylated-ERK (*P-ERK*), total-ERK (*T-ERK*), phosphorylated-MEK (*P-MEK*), total-MEK (*T-MEK*), and glyceraldehyde 3-phosphate dehydrogenase (GAPDH). **(C)** Enzymatic activity of 6PGD was assayed following the manufacturer's instructions. In brief, cell samples were lysed using assay buffer, mixed with the reaction mix, and absorbance was measured at 460 nm in kinetic mode for 60 minutes at 37°C. **(D)** Representative images of VSMC migration in the transwell assays and quantitation. **(E)** Quantitation of VSMC proliferation after si-6PGD or SCR treatment, with or without PDGF-BB stimulation. **(F)** Quantitative polymerase chain reaction analysis of messenger RNA levels of VSMC differentiation marker α smooth muscle actin (*α-SMA*), dedifferentiation marker ALDH1A3, and inflammation marker ICAM1. The data are presented as mean ± standard deviation (n = 3-8 replicates as represented by the scatter plots), and statistical analyses were performed using one-way analysis of variance with post hoc Tukey test. *ns*, not significant. $^{*}P < .05$, $^{**}P < .01$, $^{***}P < .001$.

could be identified in the adventitia. In stark contrast, in diseased coronary artery sections with profound IH lesions, prominent upregulation of 6PGD expression (staining intensity) could be observed readily in the neointimal and medial layers (Fig 1, *B*). Negative staining without primary antibody confirmed the staining specificity. To confirm the cell populations associated with aberrant 6PGD expression, we further conducted fluorescent co-staining of VSMC marker (α smooth muscle actin [α-SMA]) and 6PGD in human tissue specimens (Fig 1, *C*). Indeed, Confocal microscopy revealed extensive accumulation of phenotypically switched VSMC in the neointimal layer (IH). Aberrant 6PGD expression was observed to occur primarily in these phenotypically switched VSMC, which express less α-SMA (a hallmark of dedifferentiation). Taken together, our results indicated that the 6PGD protein level was elevated aberrantly in human coronary

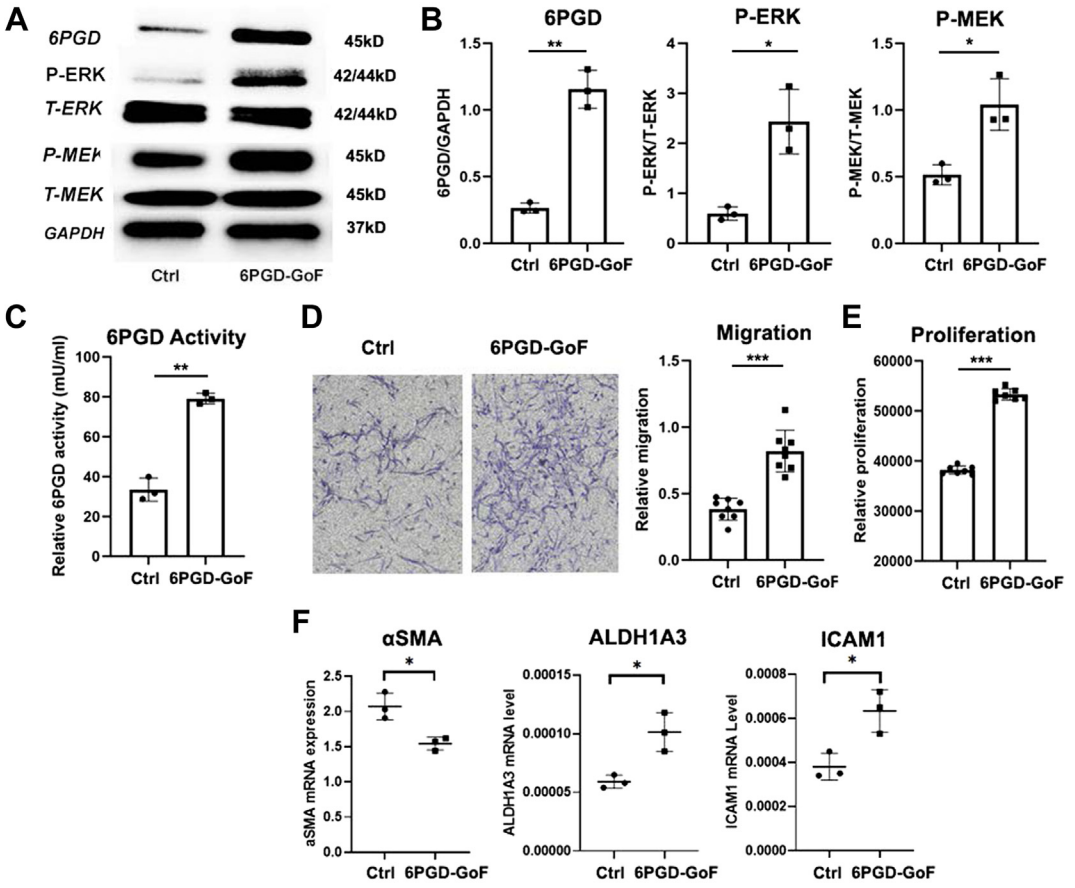

Fig 3. dCas9-mediated 6-phosphogluconate dehydrogenase (*6PGD*) transcriptional activation aggravates the hyperproliferative and migratory phenotypic switching of vascular smooth muscle cells (VSMCs) in vitro. Human aortic smooth muscle cells (AoSMCs) were subjected to serum starvation for 24 hours before transfection with lentiviral vectors expressing dCas9-SAM and gRNAs to achieve targeted transcriptional gain-of-function (*6PGD-GoF*) of 6PGD vs scrambled guide RNA control (*Ctrl*). At 48 hours after transfection, cells were collected for the downstream assays. **(A** and **B)** Representative Western blot images and protein-level quantitation of phosphorylated-ERK (*P-ERK*), total-ERK (*T-ERK*), phosphorylated-MEK (*P-MEK*), total-MEK (*T-MEK*), and 6PGD activity. **(C)** Enzymatic activity of 6PGD. **(D)** Representative images of VSMC migration in the Transwell assays and quantitation. **(E)** Quantitation of VSMC proliferation following 6PGD GoF or Ctrl treatment, with or without platelet-derived growth factor (PDGF-BB) stimulation. **(F)** Quantitative polymerase chain reaction analysis of messenger RNA levels of VSMC differentiation marker α smooth muscle actin (*α-SMA*), dedifferentiation marker ALDH1A3, and inflammation marker ICAM1. The data are presented as mean ± standard deviation (n ≥ 3 replicates as represented by the scatter plots), and statistical analyses were performed using the Student *t* test. $^{*}P < .05$, $^{**}P < .01$, $^{***}P < .001$.

arteries with IH lesions, suggesting a potential role in IH development.

6PGD loss-of-function mitigates, while its gain-of-function aggravates, the hyperproliferative and migratory phenotypic switching of VSMC *in vitro*. To mimic the pathophysiology of postangioplasty vascular responses, we treated primary human AoSMC with platelet-derived growth factor (PDGF-BB) to induce phenotypic switching as widely demonstrated. Similar to our observations in human coronary arteries with IH lesions, PDGF-BB stimulation led to profound increase in both 6PGD protein expression as well as enzymatic activity (Figs 2, *A-C*, and 3, *A-C*) in AoSMC. These observations were paralleled by increased transwell migration (Figs 2, *D*, and 3, *D*) and proliferation (Figs 2, *E*, and 3, *E*), as well as a decrease in VSMC differentiation markers (α-SMA and calponin) expression (Figs 2, *F*, and , 3, *F*, at the mRNA level' Supplementary Figs 1 and 2 (online only) at the protein level) and concomitant induction of inflammation and dedifferentiation based on ICAM1 and ALDH1A3 expressions, respectively (Figs 2, *F*, and 3, *F*), as established in our recent study.[32] We further observed the activation of the ERK/MEK signaling (Figs 2, *A-B*, and 3, *A-B*), which is implicated critically in VSMC phenotypic switching.

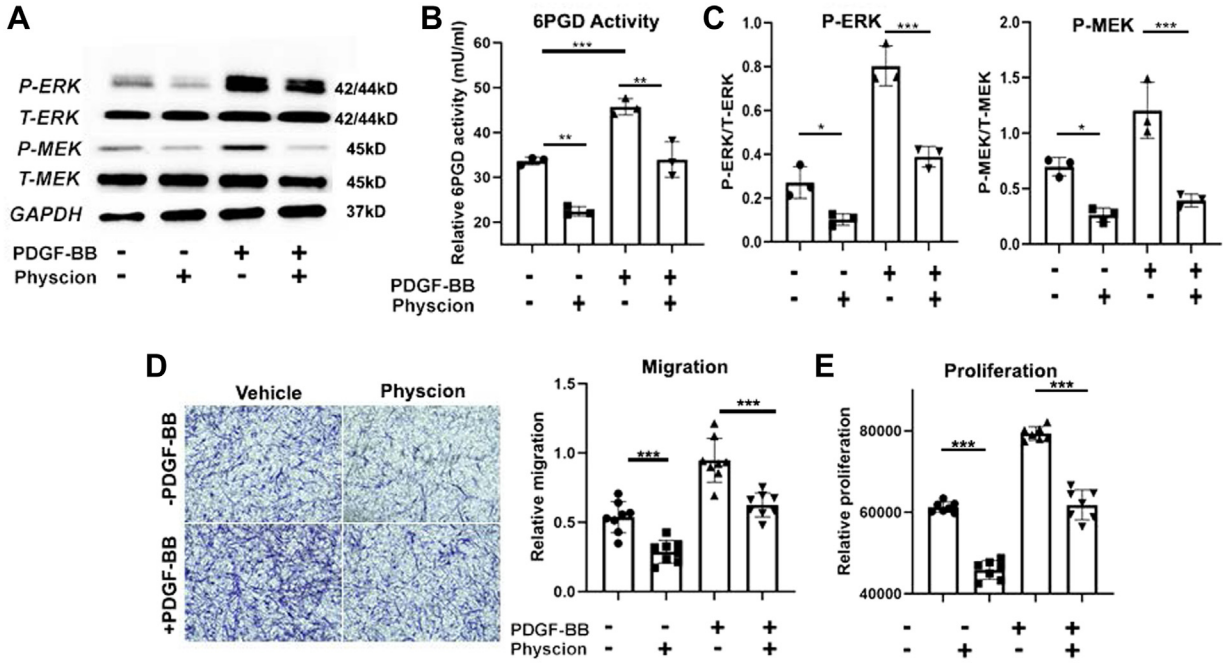

Fig 4. Small molecular inhibitor *Physcion* treatment phenocopies 6-phosphogluconate dehydrogenase (*6PGD*) loss-of-function against vascular smooth muscle cell (VSMC) phenotypic switching in vitro. Human aortic smooth muscle cells (AoSMCs) underwent serum starvation for 24 hours before treatment with *Physcion* or DMSO vehicle control. After 24 hours of treatment with *Physcion* (100 nM) or control, platelet-derived growth factor (*PDGF-BB*) was introduced to induce VSMC's hyperproliferative and migratory phenotypic switching for an additional 24 hours. **(A)** Representative Western blot images of phosphorylated-ERK (*P-ERK*), total-ERK (*T-ERK*), phosphorylated-MEK (*P-MEK*), and total-MEK (*T-MEK*). **(B)** Enzymatic activity of 6PGD. **(C)** Protein quantitation of P-ERK and P-MEK (normalized to T-ERK and T-MEK, respectively). **(D)** Representative images of VSMC migration in the Transwell assays and quantitation. **(E)** Quantitation of VSMC proliferation following *Physcion* or vehicle control treatment, with or without PDGF-BB stimulation. The data is presented as mean ± standard deviation (n ≥ 3 replicates), and statistical analysis was performed using one-way analysis of variance with post hoc Tukey test. $^{*}P < .05$, $^{**}P < .01$, $^{***}P < .001$.

To unambiguously dissect the role of 6PGD in VSMC phenotypic switching, we resorted to both loss-of-function (with 6PGD-specific siRNA) and gain-of-function (with dCas9-synergistic activation mediator-mediated transcriptional activation) approaches in vitro. After validation of successful 6PGD silencing (Fig 2, *B-C*) and transcriptional activation (Fig 3, *B-C*), we examined the proliferation, migration, dedifferentiation, and inflammation (Figs 2, *D-F*, and 3, *D-F*) of AoSMCs, as well as the status of the ERK/MEK signaling (Figs 2, *B*, and 3, *B*). Consistent with our hypothesis, we found that 6PGD silencing mitigated, whereas its transcriptional activation exacerbated the hyperproliferative, migratory, dedifferentiated, and inflammatory phenotypic switching of VSMCs, as well as the activation of the downstream ERK/MEK pathway (Figs 2, *D-F*, and 3, *D-F*). Interestingly, the changes in 6PGD status had minimal impacts on VSMC apoptosis (Supplementary Figs 1, *C-D*, and 2, *C-D*, online only), which is also implicated in the development of IH.

Administration of *Physcion* phenocopies 6PGD loss-of-function against VSMC phenotypic switching *in vitro*. Inspired by the disease-driving role of aberrant 6PDG upregulation in VSMC phenotypic switching, we hypothesized whether 6PDG would present a new actionable target for pharmacological therapy against IH. Herein, we applied *Physcion* (100 nM), a recently identified selective inhibitor of 6PGD, to PDGF-BB-stimulated VSMCs in vitro and explored its impact on VSMC phenotypic switching and downstream signaling. Consistent with our prior observations, PDGF-BB led to robust activation of 6PGD enzymatic activity, which was blocked upon *Physcion* treatment (Fig 4, *A*). Similarly, pharmacological inhibition of 6PGD with *Physcion* prevented PDGF-BB-induced AoSMC transwell migration (Fig 4, *D*), proliferation (Fig 4, *E*), and loss of VSMC differentiation markers, α-SMA and calponin (Supplementary Fig 3, *A-B*, online only). Interestingly, *Physcion* treatment elicited a marginal increase in VSMC apoptosis, albeit not statistically significant (Supplementary Fig 3, *C-D*, online

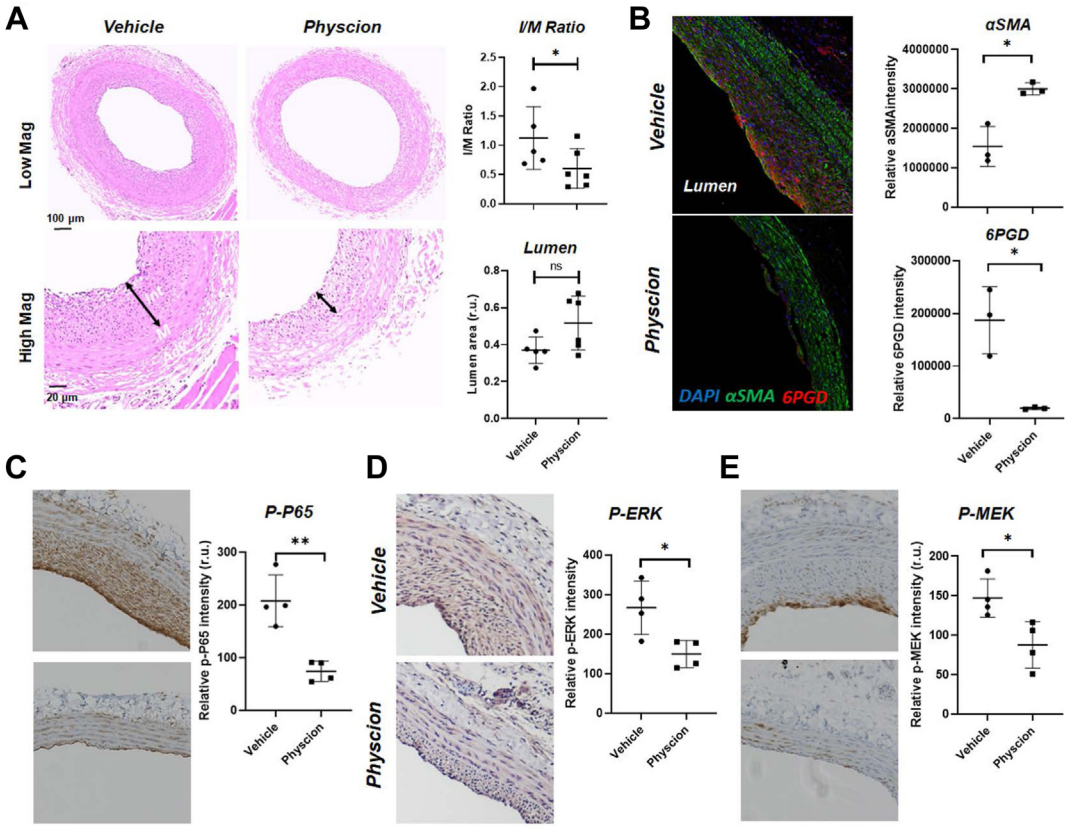

Fig 5. Perivascular administration of *Physcion* (selective 6-phosphogluconate dehydrogenase [*6PGD*] inhibitor) mitigates intimal hyperplasia (IH) in a rat model of carotid artery balloon angioplasty in vivo. Rat carotid artery balloon angioplasty was performed followed by periadventitial administration of *Physcion* (10 mg/kg) or vehicle control (equal amount of dimethylformamide) suspended in Pluronic hydrogel. The animals were euthanized 14 days later, and the arteries were collected for histological analyses. **(A)** Representative image of hematoxylin and eosin-stained carotid artery cross sections and the quantification of the intima vs media area ratio (I/M, a measure of IH) and Lumen area. **(C-E)** Representative images and quantitation of immunohistochemical staining with antibodies specific to P-P65 **(C)**, phosphorylated-ERK (*P-ERK*) **(D)**, and phosphorylated-MEK (*P-MEK*) **(E)**. n = 4-5 animals, Student *t* test. $^{*}P < .05$, $^{**}P < .01$, $^{***}P < .001$. A pair of arrows define the neointima thickness. Tunica intima (*Int*), media (*M*), and adventitia (*Adv*) are annotated.

only). Finally, *Physcion* treatment decreased the phosphorylation of the prosurvival, promigratory, and dedifferentiated ERK/MEK pathway (Fig 4, *C*), phenocopying 6PGD silencing (Fig 2, *A*). Collectively, these in vitro findings suggest that *Physcion* may serve as a viable therapeutic agent to target the aberrant 6PGD activation/upregulation and, consequently, VSMC phenotypic switching.

Perivascular administration of *Physcion* (6PGD inhibitor) mitigates IH in a rat carotid artery balloon angioplasty model in vivo. To determine the in vivo implication of 6PGD blockade, we resorted to 6PGD, a selective inhibitor to 6PGD, for hydrogel-assisted perivascular delivery as described in Methods section. At day 14 after angioplasty, carotid arteries were collected for histological and morphometric analyses. As shown in Fig 5, *A*, balloon angioplasty led to the consistent development of IH in the vehicle control group, as evidenced by the formation of neointima beyond the IEL and decreased luminal patency. However, upon perivascular treatment with 6PGD inhibitor *Physcion*, IH was significantly reduced, as evidenced by a decreased I/M ratio, albeit the numerical increase in luminal patency was not statistically significant. Hallmarks of VSMC phenotypic switching, such as loss of α-SMA (dedifferentiation) and increased phosphorylation of p65 as part of the nuclear factor-κB signaling (inflammation), were also rescued upon pharmacological inhibition of 6PGD (Fig 5, *B-C*). Interestingly, although *Physcion* only blocks the enzymatic activities of 6PGD, we still observed a significant reduction in the overall expression level of 6PGD in carotid arteries from *Physcion*-treated animals (Fig 5, *B*, and Supplementary Fig 4, *A*, online only). Additionally,

localized *Physcion* treatment phenocopied 6PGD loss-of-function in vitro, resulting in effective inhibition of the pro-VSMC phenotypic switching ERK/MEK signaling (Fig 5, *D-E*). Collectively, our data suggests a potential role of pharmacologically targeting 6PGD in the development of next-generation antirestenotic therapies.

DISCUSSION

In this study, we report the first experimental evidence supporting a potential role of 6PGD, one of the three enzymes in the PPP metabolic pathway, in driving SMC phenotypic switching in the context of IH. Using clinical and experimental specimens of arteries with or without IH, we observed robust upregulation of 6PGD expression in the phenotypically switched SMC, particularly in the neointima lesions. Similarly, 6PGD activity and protein expression were profoundly stimulated upon PDGF-BB-induced VSMC phenotypic switching. Using gain-(dCas9-mediated transcriptional activation) and loss-of-function (siRNA-mediated silencing), we were able to demonstrate the pathogenic role of 6PGD in driving VSMC hyperproliferation, migration, and dedifferentiation while exerting minimal impact on VSMC apoptosis. Mechanistically, we identified the MEK/ERK pathway as a possible downstream signaling behind 6PGD's pathophysiological role in VSMC. Finally, via perivascular localized delivery of *Physcion*, a selective 6PGD inhibitor with poor systemic bioavailability, we achieved effective mitigation of IH in a rat model of balloon angioplasty in carotid arteries. Collectively, we contend that aberrant 6PGD expression and activity—indicative of a metabolic shift toward PPP—could serve as a new disease-driving mechanism and hence an actionable target for the development of effective new therapies for IH and restenosis after endovascular interventions.

Cardiovascular and peripheral vascular diseases remain the leading causes of mortality and morbidity globally. Currently, endovascular interventions are the treatment of choice in a large portion of those patients; however, the long-term outcomes have been plagued by restenosis. Recent innovations in local drug delivery approaches, such as drug-coated balloons and drug-eluting stents, have demonstrated improved clinical outcomes over bare metal stents and plain balloons. Nonetheless, resistant restenosis and de novo neoatherosclerosis remain an unsolved issue; to make things worse, the increased risk of severe complications (eg, thrombosis, drug/polymer wash-out into circulation) further testify to the need for new therapeutic paradigms. The currently used antirestenotic drugs are mostly cytotoxic and/or cytostatic agents (ie, paclitaxel, sirolimus) with established toxicities, both locally and systemically. Despite collective ongoing efforts from researchers worldwide to actively uncover new druggable disease-driving or -inhibiting mechanisms behind VSMC phenotypic switching, thus far none of their respective inhibitors or agonists have demonstrated clinical usefulness successfully. Our current study aims to uncover a hitherto unexplored actionable enzyme target, 6PGD, that could be used via readily available selective inhibitors to block the hyperproliferative and migratory VSMCs from fueling the development of IH and, ultimately, restenosis.

Metabolic shift, or bioenergetic reprogramming, has been increasingly recognized to play a critical role in dictating cellular phenotypes. In recent years, experimental evidence derived from VSMC-specific lineaging tracing, multi-omics approaches, and transgenic models have uncovered the fine balance between oxidative phosphorylation and glycolysis as a key player in VSMC phenotypic modulation.[33] For example, genetic deletion of pyruvate kinase M isoform 2 the rate-limiting glycolytic enzyme responsible for the last step of glycolysis, effectively reversed the hyperproliferative and migratory phenotypic switching of VSMC and wire injury-induced IH in murine carotid arteries.[11,13] Similarly, adenoviral overexpression of lactate dehydrogenase A, which catalyzes the pyruvate-to-lactate conversion in glycolysis, promoted VSMC phenotypic switching and IH in vivo.[34] In contrast, promoting the metabolic shift toward oxidative phosphorylation, as demonstrated by Yiting Jia et al via PKM isoform 2 to isoform 1 conversion, could maintain the phenotypic integrity of VSMC and prevent wire injury-induced IH in mice.[35] However, our current understanding of PPP's participation in VSMC phenotypic switching and IH is extremely limited. Metabolomic data derived from cultured VSMCs, albeit from pulmonary arteries, revealed a shift of glucose flux to PPP under hyperproliferative phenotypic switching.[15] Similarly, as shown by Peiró et al[16] in cultured human aortic VSMC, co-stimulation with high glucose and inflammatory cytokine led to overactivation of PPP, concomitant with disturbed redox homeostasis. Kitagawa et al[14] demonstrated that loss of function of G6PD (G6PD^{S188F}), the speed-limiting enzyme of PPP, could prevent VSMC's dedifferentiated phenotypic switching partially, corroborating epidemiological findings of a lesser prevalence of vascular diseases in G6PD^{S188F} carriers. Clearly, there is an unmet need to extend our understanding of the PPP metabolism and clarify its pathophysiological implications in VSMC and vascular diseases.

To the best of our knowledge, our current study offers the first experimental insights into the potential disease-driving role of 6PGD in VSMC phenotypic switching and IH. In fact, only two existing studies have mentioned 6PGD in the cardiovascular system. As mentioned, Tomas et al[18] conducted an unbiased metabolomics and transcriptomics profiling of stable vs unstable atherosclerotic plaques from archived endarterectomies, leading to the discovery of numerous metabolism pathways with potential diagnostic and prognostic significances which include 6PGD and PPP. In a recent developmental study using zebrafish and

mouse embryos, 6PGD loss of function in endothelial cells alone could disrupt the elastogenesis and vascular mural cell (including VSMC) coverage of dorsal aorta, suggesting a more nuanced role of 6PGD under physiological/developmental vs diseased state.[36] In pursuit of the potential downstream signaling cascade, our study further demonstrates that aberrant increase in 6PGD expression and activity could lead to downstream activation of the ERK/MEK pathway, which has been established by our group and others to drive VSMC phenotypic switching directly, as well as the pathogenesis of IH.[32,37-40] Although the exact mode of action remains to be further interrogated, it is likely that the 6PGD-ERK/MEK cascade is caused by the aberrant accumulation of metabolites as a result of the glucose metabolic shunt that is PPP. By entering into PPP instead of glycolysis, glucose-6-phosphate will be ultimately converted to ribulose-5-phosphate (directly by 6PGD) and ultimately ribose-5-phosphate, which are the building blocks for purine and pyrimidine biosynthesis.[41-43] Consequently, excessive purine synthesis could lead to increased accumulation of metabolites that could directly (eg, cyclic guanosine monophosphate[44]) or indirectly (eg, through purinergic receptors or conversion to uric acid[45,46]) activate mitogen-activated protein kinases, including literature reports in VSMC.[47-50] Future investigations, including cellular and tissue-derived metabolomics, will help to dissect the molecular basis underlying the pro-IH role of aberrant 6PGD and PPP activation, possibly via mobilizing the MAPK pathways (eg, ERK/MEK), which are the widely established master regulators of VSMC phenotypic switching.

Pharmacotherapies targeting 6PGD and PPP offer new opportunities for the treatment of a wide range of diseases. Indeed, a growing body of evidence points to a disease-driving role of aberrant 6PGD activation and upregulation in malignancies, ranging from tumorigenesis and chemoresistance to cancer metastasis.[51-54] Under physiological conditions, 6PGD also plays pivotal roles in upkeeping the energy expenditures as well as glutathione reduction in cell types that are highly dependent on PPP, such as regulatory T cells and erythrocytes.[55,56] Recent drug screening efforts led to the identification of *Physcion*, a naturally occurring anthraquinone derivative commonly found in Rhubarb, and its derivative, S3, as a potent PPP inhibitor selective to 6PGD but not to G6PD.[41] Indeed, therapeutic agents targeting 6PGD and PPP in general have demonstrated potential utilities in various types of tumors in murine models, capitalizing on tumor cells' metabolic shifting and "addiction" to PPP as similarly observed in VSMC.[57-59] Notwithstanding the promising preclinical benefits, *Physcion* and all 6PGD inhibitors could interfere with other signaling pathways, as is the case for most naturally occurring small molecule compounds with promiscuous targets or modes of action. It is worth noting that *Emodin*, which shares structural similarity with *Physcion* (both derived from Rhubarb), has also been demonstrated with in vitro and in vivo benefits against VSMC phenotypic switching and IH, although Emodin's direct inhibition of 6PGD.[60] In the current proof-of-concept study, we resorted to *Physcion* as the model drug to test the early therapeutic potential in our rat model. Future efforts, such as tissue specific transgenic animals with 6PGD gain- or loss-of-functions, will offer more clarity over the exact contribution of 6PGD to IH in vivo.

Key obstacles remain to be addressed for future translation of therapies targeting 6PGD and PPP to patient care. First is the delivery approach. Like most anthraquinones, *Physcion* suffers from poor bioavailability, solubility, systemic toxicity, and so on, which greatly diminishes the enthusiasm behind its clinical translation.[61] Herein, we used the Food and Drug Administration-approved, biocompatible F127 Pluronic hydrogel with a 2- to 3-day release profile for the localized delivery of *Physcion*, hence bypassing all the aforementioned obstacles. However, for endovascular applications, different approaches are needed to accommodate for device-mediated (eg, drug-eluting stents and drug-coated balloons) and targeted, systemic delivery (eg, nanoparticle-assisted injectables or oral formulations of *Physcion*). Another potential concern is the systemic complications as a consequence of PPP blockade. Indeed, deficiencies in PPP enzymes, such as G6PD (highly prevalent, 400 million affected worldwide) and 6PGD (rare), have been linked tightly to the development of hemolytic anemia, owing to erythrocyte's dependence on PPP for bioenergetics.[62-64] Thus far, no evidence supports such adverse effects for *Physcion* and other PPP inhibitors in rodent models. Interestingly, one study reported that *Physcion* at extremely high concentrations (50-100 μM in contrast with 100 nM used in our study) could induce hemolysis in isolated erythrocytes ex vivo, although its relevance to in vivo scenarios is low.[65] Nevertheless, cautious should be exercised for future development of 6PGD and PPP-targeting therapies in lights of the potential systemic complications, which, coincidentally, could be addressed with advancement in targeted delivery approaches.

There are several limitations associated with our current study. First, our in vitro study used primary human VSMCs isolated from the aorta, differing from the anatomical locations in our rodent study (carotid artery) and clinical practice (coronary and peripheral arteries). In lieu of experimental validation in VSMC from arterial origins (coronary, carotid, femoral/iliac, etc), the generality of our observation concerning 6PGD's role in vitro may be limited; recent evidence points to an anatomical origin-based distinctions in VSMC phenotypes in health and disease.[66] Second, although both loss- and gain-of-function approaches were adopted to probe our hypothesis in vitro, the in vivo evidence was derived solely from pharmacological inhibition using a selective small

molecular compound. VSMC-specific transgenic approaches (eg, conditional knockout mice, tissue-specific lentivirus-mediated shRNA transduction), instead of pharmacological antagonism, could offer more precision to dissect the exact cellular and molecular contributions. Third, our in vivo model lacks primary atherosclerotic lesions before angioplasty, contrasting the clinical scenario where the target vessel lumens undergo a secondary narrowing (hence the term restenosis). Additionally, owing to the scope of the study, we did not determine the intracellular level of intermediate metabolites for glycolysis and PPP upon the in vitro experimental treatment. Finally, we acknowledge that it remains to be determined as to what constitutes the upstream regulatory mechanism behind 6PGD's aberrant upregulation in expression and activity. Future studies are warranted to address these limitations.

CONCLUSIONS

Our current study unveiled a disease driving role of the PPP metabolic enzyme 6PGD in promoting VSMC's hyperproliferative and migratory phenotypic switching, possibly via mobilizing the ERK/MEK signaling. Not only is the aberrant upregulation of 6PGD expression robustly observed in IH from patient-derived coronary arterial lesions, but also activation or silence of this enzyme could exacerbate or inhibit PDGF-BB-induced VSMC phenotypic switching. Moreover, localized delivery of a selective 6PGD inhibitor, *Physcion*, effectively mitigated the development of IH following endovascular injury with balloon angioplasty in a rat model. These findings expand our understanding of a much lesser explored metabolic pathway in VSMC biology and offer a new actionable target for the development of next-generation antirestenotic drug-eluting devices.

DISCLOSURES

Supported by the National Institutes of Health (R01HL162895 [to B.W.]) and by Veteran's Administration (VA Merit Review, BX001792 [to C.E.C.], VA Merit Review award, BX 006063 [C.E.C.], and a Senior Research Career Scientist Award, IK6BX004603 [to C.E.C.]). This work was peripherally supported by way of research cores, methodology and technology development, and software development by the National Institutes of Health by way of P01 CA171983 (Project 1 to C.E.C.) and the R01s AI139072 (to C.E.C.) and GM137578 (to C.E.C.). The contents of this manuscript do not represent the views of the Department of Veterans Affairs or the United States Government.

REFERENCES

1. Buccheri D, Piraino D, Andolina G, Cortese B. Understanding and managing in-stent restenosis: a review of clinical data, from pathogenesis to treatment. *J Thorac Dis*. 2016;8:E1150—E1162.
2. de Donato G, Setacci F, Mele M, Giannace G, Galzerano G, Setacci C. Restenosis after coronary and peripheral intervention: efficacy and clinical impact of Cilostazol. *Ann Vasc Surg*. 2017;41:300—307.
3. Déglise S, Bechelli C, Allagnat F. Vascular smooth muscle cells in intimal hyperplasia, an update. *Front Physiol*. 2022;13:1081881.
4. Smith SA, Newby AC, Bond M. Ending restenosis: inhibition of vascular smooth muscle cell proliferation by cAMP. *Cells*. 2019;8:1447.
5. Jawien A, Bowen-Pope DF, Lindner V, Schwartz SM, Clowes AW. Platelet-derived growth factor promotes smooth muscle migration and intimal thickening in a rat model of balloon angioplasty. *J Clin Invest*. 1992;89:507—511.
6. Lu H, Du W, Ren L, Hamblin MH, Becker RC, Chen YE, Fan Y. Vascular smooth muscle cells in aortic aneurysm: from genetics to mechanisms. *J Am Heart Assoc*. 2021;10:e023601.
7. Bennett MR, Sinha S, Owens GK. Vascular smooth muscle cells in atherosclerosis. *Circ Res*. 2016;118:692—702.
8. Yodsanit N, Shirasu T, Huang Y, et al. Targeted PERK inhibition with biomimetic nanoclusters confers preventative and interventional benefits to elastase-induced abdominal aortic aneurysms. *Bioact Mater*. 2023;26:52—63.
9. Zhang X, Zheng B, Zhao L, et al. KLF4-PFKFB3-driven glycolysis is essential for phenotypic switching of vascular smooth muscle cells. *Commun Biol*. 2022;5:1332.
10. Newman AAC, Serbulea V, Baylis RA, et al. Multiple cell types contribute to the atherosclerotic lesion fibrous cap by PDGFRβ and bioenergetic mechanisms. *Nat Metab*. 2021;3:166—181.
11. Jain M, Dhanesha N, Doddapattar P, et al. Smooth muscle cell-specific PKM2 (pyruvate kinase muscle 2) promotes smooth muscle cell phenotypic switching and neointimal hyperplasia. *Arterioscler Thromb Vasc Biol*. 2021;41:1724—1737.
12. Perez J, Hill BG, Benavides GA, Dranka BP, Darley-Usmar VM. Role of cellular bioenergetics in smooth muscle cell proliferation induced by platelet-derived growth factor. *Biochem J*. 2010;428:255—267.
13. Yang L, Gao L, Nickel T, et al. Lactate promotes synthetic phenotype in vascular smooth muscle cells. *Circ Res*. 2017;121:1251—1262.
14. Kitagawa A, Kizub I, Jacob C, et al. CRISPR-mediated single nucleotide polymorphism modeling in rats reveals insight into reduced cardiovascular risk associated with Mediterranean G6PD variant. *Hypertension*. 2020;76:523—532.
15. Alamri A, Burzangi AS, Coats P, Watson DG. Untargeted metabolic profiling cell-based approach of pulmonary artery smooth muscle cells in response to high glucose and the effect of the antioxidant vitamins D and E. *Metabolites*. 2018;8:87.
16. Peiró C, Romacho T, Azcutia V, et al. Inflammation, glucose, and vascular cell damage: the role of the pentose phosphate pathway. *Cardiovasc Diabetol*. 2016;15:82.
17. Dhagia V, Kitagawa A, Jacob C, et al. G6PD activity contributes to the regulation of histone acetylation and gene expression in smooth muscle cells and to the pathogenesis of vascular diseases. *Am J Physiol Heart Circ Physiol*. 2021;320:H999—H1016.
18. Tomas L, Edsfeldt A, Mollet IG, et al. Altered metabolism distinguishes high-risk from stable carotid atherosclerotic plaques. *Eur Heart J*. 2018;39:2301—2310.
19. Sakamoto A, Kawakami R, Mori M, et al. CD163+ macrophages restrain vascular calcification, promoting the development of high-risk plaque. *JCI Insight*. 2023;8.
20. Zhang M, Li J, Wang Q, et al. Gene-repressing epigenetic reader EED unexpectedly enhances cyclinD1 gene activation. *Mol Ther Nucleic Acids*. 2023;31:717—729.
21. Xie X, Shirasu T, Li J, Guo LW, Kent KC. miR579-3p is an inhibitory modulator of neointimal hyperplasia and transcription factors c-MYB and KLF4. *Cell Death Discov*. 2023;9:73.
22. Xie X, Guo LW, Kent CK. miR548ai antagonism attenuates exosome-induced endothelial cell dysfunction. *Cell Death Discov*. 2021;7:318.
23. Zhang M, Urabe G, Ozer HG, et al. Angioplasty induces epigenomic remodeling in injured arteries. *Life Sci Alliance*. 2022;5:e202101114.
24. Xie X, Urabe G, Marcho L, Williams C, Guo LW, Kent KC. Smad3 regulates Neuropilin 2 transcription by Binding to its 5' Untranslated region. *J Am Heart Assoc*. 2020;9:e015487.
25. National Research Council. *Guide for the Care and Use of Laboratory Animals*. 8th ed. The National Academies Press; 2011. https://doi.org/10.17226/12910. Accessed September 9, 2024. https://nap.nationalacademies.org/catalog/12910/guide-for-the-care-and-use-of-laboratory-animals-eighth.
26. Zhao Y, Shirasu T, Yodsanit N, et al. Biomimetic, ROS-detonable nanoclusters - a multimodal nanoplatform for anti-restenotic therapy. *J Control Release*. 2021;338:295—306.

27. Yin L, Tong Y, Husain Z, et al. Targeted NAD+ Delivery for intimal Hyperplasia and Re-endothelialization: a novel anti-restenotic therapy approach. *bioRxiv*. 2024:2024.02.20.581249.
28. Guo LW, Wang B, Goel SA, et al. Halofuginone stimulates adaptive remodeling and preserves re-endothelialization in balloon-injured rat carotid arteries. *Circ Cardiovasc Interv*. 2014;7:594–601.
29. Wang B, Zhang M, Takayama T, Shi X, Roenneburg DA, Kent KC, Guo LW. BET Bromodomain blockade mitigates intimal hyperplasia in rat carotid arteries. *EBioMedicine*. 2015;2:1650–1661.
30. Zhang M, Urabe G, Little C, et al. HDAC6 regulates the MRTF-A/SRF axis and vascular smooth muscle cell Plasticity. *JACC Basic Transl Sci*. 2018;3:782–795.
31. Shirasu T, Yodsanit N, Xie X, et al. An adventitial painting modality of local drug delivery to abate intimal hyperplasia. *Biomaterials*. 2021;275:120968.
32. Xie X, Urabe G, Marcho L, Stratton M, Guo LW, Kent CK. ALDH1A3 regulations of matricellular proteins promote vascular smooth muscle cell proliferation. *iScience*. 2019;19:872–882.
33. Sun X, Wu J, Zhang X, et al. Atlas of cell repertoire within neointimal lesions is metabolically altered in hypertensive rats. *Hypertension*. 2024;81:787–800.
34. Chen ZH, Cao SH, Ren ZY, et al. LDHA maintains the growth and migration of vascular smooth muscle cells and promotes neointima formation via crosstalk between K5 crotonylation and K76 mono-ubiquitination. *bioRxiv*. 2023:2023.02.28.530389.
35. Jia Y, Mao C, Ma Z, et al. PHB2 maintains the contractile phenotype of VSMCs by counteracting PKM2 Splicing. *Circ Res*. 2022;131:807–824.
36. Facchinello N, Astone M, Audano M, et al. Oxidative pentose phosphate pathway controls vascular mural cell coverage by regulating extracellular matrix composition. *Nat Metab*. 2022;4:123–140.
37. Sakakibara K, Kubota K, Worku B, et al. PDGF-BB regulates p27 expression through ERK-dependent RNA turn-over in vascular smooth muscle cells. *J Biol Chem*. 2005;280:25470–25477.
38. Gennaro G, Ménard C, Michaud SE, Deblois D, Rivard A. Inhibition of vascular smooth muscle cell proliferation and neointimal formation in injured arteries by a novel, oral mitogen-activated protein kinase/extracellular signal-regulated kinase inhibitor. *Circulation*. 2004;110:3367–3371.
39. Zhang M, Fraser D, Phillips A. ERK, p38, and Smad signaling pathways differentially regulate transforming growth factor-beta1 autoinduction in proximal tubular epithelial cells. *Am J Pathol*. 2006;169:1282–1293.
40. Suwanabol PA, Seedial SM, Shi X, et al. Transforming growth factor-β increases vascular smooth muscle cell proliferation through the Smad3 and extracellular signal-regulated kinase mitogen-activated protein kinases pathways. *J Vasc Surg*. 2012;56:446–454.
41. Lin R, Elf S, Shan C, et al. 6-Phosphogluconate dehydrogenase links oxidative PPP, lipogenesis and tumour growth by inhibiting LKB1-AMPK signalling. *Nat Cell Biol*. 2015;17:1484–1496.
42. Grucela PK, Fuhrer T, Sauer U, Chao Y, Zhang YE. Ribose 5-phosphate: the key metabolite bridging the metabolisms of nucleotides and amino acids during stringent response in Escherichia coli? *Microb Cell*. 2023;10:141–144.
43. De Vitto H, Arachchige DB, Richardson BC, French JB. The intersection of purine and mitochondrial metabolism in cancer. *Cells*. 2021;10:2603.
44. Lv Y, Wang X, Li X, et al. Nucleotide de novo synthesis increases breast cancer stemness and metastasis via cGMP-PKG-MAPK signaling pathway. *PLoS Biol*. 2020;18:e3000872.
45. Huang Z, Xie N, Illes P, et al. From purines to purinergic signalling: molecular functions and human diseases. *Signal Transduct Target Ther*. 2021;6:162.
46. Kimura Y, Tsukui D, Kono H. Uric acid in inflammation and the pathogenesis of atherosclerosis. *Int J Mol Sci*. 2021;22:12394.
47. Li H, Qian F, Liu H, Zhang Z. Elevated uric acid levels promote vascular smooth muscle cells (VSMC) proliferation via an Nod-Like receptor protein 3 (NLRP3)-Inflammasome-Dependent mechanism. *Med Sci Monit*. 2019;25:8457–8464.
48. Martin-Aragon Baudel M, Espinosa-Tanguma R, Nieves-Cintron M, Navedo MF. Purinergic signaling during Hyperglycemia in vascular smooth muscle cells. *Front Endocrinol*. 2020;11:329.
49. Chaulet H, Desgranges C, Renault MA, et al. Extracellular nucleotides induce arterial smooth muscle cell migration via osteopontin. *Circ Res*. 2001;89:772–778.
50. Ma Q, Yang Q, Xu J, et al. ATIC-associated de novo purine synthesis is critically involved in proliferative arterial disease. *Circulation*. 2022;146:1444–1460.
51. Chen C, Du P, Zhang Z, Bao D. 6-Phosphogluconate dehydrogenase inhibition arrests growth and induces apoptosis in gastric cancer via AMPK activation and oxidative stress. *Open Life Sci*. 2023;18:20220514.
52. Sarfraz I, Rasul A, Hussain G, et al. 6-Phosphogluconate dehydrogenase fuels multiple aspects of cancer cells: from cancer initiation to metastasis and chemoresistance. *Biofactors*. 2020;46:550–562.
53. Chen H, Wu D, Bao L, Yin T, Lei D, Yu J, Tong X. 6PGD inhibition sensitizes hepatocellular carcinoma to chemotherapy via AMPK activation and metabolic reprogramming. *Biomed Pharmacother*. 2019;111:1353–1358.
54. Zheng W, Feng Q, Liu J, et al. Inhibition of 6-phosphogluconate dehydrogenase reverses cisplatin resistance in ovarian and lung cancer. *Front Pharmacol*. 2017;8:421.
55. Daneshmandi S, Cassel T, Higashi RM, Fan TWM, Seth P. 6-Phosphogluconate dehydrogenase (6PGD), a key checkpoint in reprogramming of regulatory T cells metabolism and function. *Elife*. 2021;10:e67476.
56. Vives Corrons JL, Colomer D, Pujades A, et al. Congenital 6-phosphogluconate dehydrogenase (6PGD) deficiency associated with chronic hemolytic anemia in a Spanish family. *Am J Hematol*. 1996;53:221–227.
57. Elf S, Lin R, Xia S, et al. Targeting 6-phosphogluconate dehydrogenase in the oxidative PPP sensitizes leukemia cells to antimalarial agent dihydroartemisinin. *Oncogene*. 2017;36:254–262.
58. Pang MJ, Yang Z, Zhang XL, Liu ZF, Fan J, Zhang HY. Physcion, a naturally occurring anthraquinone derivative, induces apoptosis and autophagy in human nasopharyngeal carcinoma. *Acta Pharmacol Sin*. 2016;37:1623–1640.
59. Gillis JL, Hinneh JA, Ryan NK, et al. A feedback loop between the androgen receptor and 6-phosphogluconate dehydrogenase (6PGD) drives prostate cancer growth. *Elife*. 2021;10:e62592.
60. Xu K, Al-Ani MK, Wang C, Qiu X, Chi Q, Zhu P, Dong N. Emodin as a selective proliferative inhibitor of vascular smooth muscle cells versus endothelial cells suppress arterial intima formation. *Life Sci*. 2018;207:9–14.
61. Khuda F, Zahir I, Khalil AAK, et al. Preparation, characterization, and evaluation of physcion nanoparticles for enhanced oral bioavailability: an attempt to improve its antioxidant and anticancer potential. *ACS Omega*. 2023;8:33955–33965.
62. Bubp J, Jen M, Matuszewski K. Caring for glucose-6-phosphate dehydrogenase (G6PD)-Deficient patients: implications for pharmacy. *P T*. 2015;40:572–574.
63. Caprari P, Caforio MP, Cianciulli P, et al. 6-Phosphogluconate dehydrogenase deficiency in an Italian family. *Ann Hematol*. 2001;80:41–44.
64. Luzzatto L, Ally M, Notaro R. Glucose-6-phosphate dehydrogenase deficiency. *Blood*. 2020;136:1225–1240.
65. Akiel M, Alsughayyir J, Basudan AM, et al. Physcion induces hemolysis and Premature Phosphatidylserine Externalization in human erythrocytes. *Biol Pharm Bull*. 2021;44:372–378.
66. Muhl L, Mocci G, Pietilä R, et al. A single-cell transcriptomic inventory of murine smooth muscle cells. *Dev Cell*. 2022;57:2426–2443.e6.

Submitted Apr 10, 2024; accepted Jul 21, 2024.